Cell Electrophysiology with Carbon Nanopipettes

Michael G. Schrlau,[†] Nae J. Dun,[‡] and Haim H. Bau[§,*]

[†]Department of Mechanical Engineering and Applied Mechanics, University of Pennsylvania, 229 Towne Building, 220 South 33rd Street, Philadelphia, Pennsylvania 19104, [‡]Department of Pharmacology, Temple University, School of Medicine, 3400 North Broad Street, MRB Rm 324, Philadelphia, Pennsylvania 19140, and [§]Department of Mechanical Engineering and Applied Mechanics, University of Pennsylvania, 229 Towne Building, 220 South 33rd Street, Philadelphia, Pennsylvania 19104

ABSTRACT The ability to monitor living cell behavior in real time and with high spatial resolution is vital for advancing our knowledge of cellular machinery and evaluating cellular response to various drugs. Here, we report the development and utilization of carbon-based nanoelectrodes for cell electrophysiology. We employ carbon nanopipettes (CNPs), novel carbon-based nanoprobes which integrate carbon nanopipes into the tips of pulled glass capillaries, to measure electrical signals in the mouse hippocampal cell line HT-22. Using a standard electrophysiology amplifier in current-clamp mode, we measured the resting membrane potential of cells and their transient membrane response to extracellular pharmacological agents. In addition to their superior injection capabilities reported previously, CNPs are capable of multifunctionality, enabling, for example, concurrent intracellular injection and electrical measurements without damaging cells.

KEYWORDS: nanopipette · nanotube · nanoprobe · nanoelectrode · carbon · cell · electrophysiology

Cellular probes designed to monitor electrophysiological events play a crucial role in experimental cell biology and pharmacology.[1] In modern electrophysiology, electrolyte-filled glass micropipettes are utilized to access intracellular domains in order to measure how a stimulus affects the flow of ions through and/or changes the electrical potential across the cell membrane. Traditionally, electrical measurements in small cells are measured with either large-tipped, glass micropipettes filled with intracellular solution (2−3 μm OD, patch-clamp technique)[2] or fine-tipped, glass micropipettes filled with highly concentrated salt solution (<1 μm OD, sharp microelectrode technique).[3,4] Although very versatile and widely used, the patch-clamp technique ruptures the cell membrane and alters the internal milieu of a cell, preventing long-term and/or repetitive monitoring. In contrast, fine-tipped, glass microelectrodes are less intrusive and therefore are more likely to spare a cell from irreparable damage. However, cell damage may still occur during prolonged measurement when the high concentration electrolyte contained in the pipet's lumen diffuses into the cell. Problems that plague both intracellular recording techniques and inevitably degrade recording performance include clogging of the electrode tip, collecting debris at the tip during probe penetration, and damaging the tip upon approaching and penetrating the cell.[5]

Glass pipettes are typically used either for electrophysiological measurements or for injection but are not capable of performing both tasks concurrently. Recently, concurrent injection and electrical measurement was proposed with liquid-filled glass electrodes.[6] The electrical measurement is facilitated by inserting high conductivity electrolyte above the fluid to be injected. In other words, the electrical measurement would be affected by the injection process. Current glass-based technologies preclude independent electrical measurement of physiological responses during concurrent injection of molecules.

To overcome some of these shortcomings, we have developed and used hollow, ohmic nanoelectrodes for intracellular recording. Ohmic nanoelectrodes are a promising technology for cell physiology: they provide sturdy electrodes to penetrate through tissue and into cells, measure electrical signals without altering cell characteristics, and are well-suited for microfluidic-based, laboratory-on-chip platforms for high-throughput cell analysis.[7,8] For example, Yum *et al.* demonstrated electrochemical detection in small aqueous drops (10 μm in diameter) with metal, ring-shaped nanoelectrodes coated around boron nitride nanotubes.[9] Additionally, Sun *et al.* described intracellular and extracellular voltammetry with solid Pt nanoelectrodes.[10] Inspired by these two examples of

*Address correspondence to bau@seas.upenn.edu.

Received for review December 12, 2008 and accepted January 28, 2009.

Published online February 4, 2009.
10.1021/nn800851d CCC: $40.75

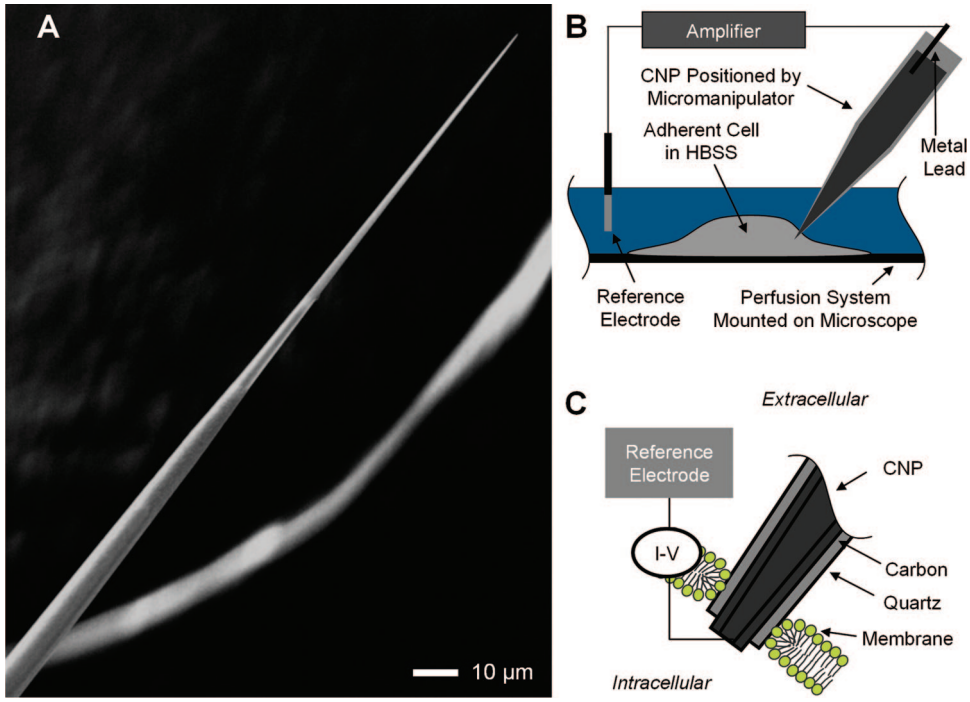

Figure 1. CNPs for electrophysiology. (A) SEM micrograph (10 kV) of a CNP tip. (B) Schematic detailing the experimental setup for CNP-based electrophysiology. CNP penetrates the cell and measures membrane potentials in current-clamp mode *versus* an Ag/AgCl reference electrode submerged in HBSS. (C) Cross-section schematic of a CNP and of the interface between the CNP and the cell membrane.

single-function, ohmic nanoelectrodes, we envisioned utilizing carbon nanotubes and nanopipes as hollow, ohmic nanoelectrodes to facilitate both intracellular delivery and electrical recording.

Ever since their discovery, researchers have been intrigued by the possibility of using carbon nanotubes and nanopipes for cell probing because of their flexible yet durable mechanical properties,[11] high electrical conductivity,[12] and functionalizable surface where proteins, DNA, or oligos can be immobilized for the detection of target analytes.[13] However, the difficulty of interfacing these nanostructures with macroscopic devices that can be easily manipulated has hampered their application for cell probing.

Our approach provides an elegant solution to this problem by facilitating the construction of integrated nanodevices without a need for assembly. Our technology employs carbon nanopipettes (CNPs) (Figure 1A,C), which integrate carbon nanopipes, with diameters ranging from tens to hundreds of nanometers and lengths ranging from hundreds of nanometers to hundreds of microns, into the tips of pulled glass capillaries.[11,14] CNPs provide an accessible, hollow, conductive, carbon-based nanochannel for simultaneous intracellular delivery and recording. CNPs are manufactured *en mass* without any assembly and fit standard cell physiology systems such as manipulators, injectors, and electrophysiology amplifiers.

CNP cellular probes have shown superior performance over their glass counterparts. Recently, we reported CNPs could penetrate cells and inject calcium-mobilizing second messengers without compromising cell viability and with fewer instances of tip clogging and breakage.[15] To investigate cell electrophysiology, we utilized a standard system, depicted schematically in Figure 1B, consisting of an electrophysiology amplifier, a micromanipulator, and an upright microscope with a water-immersion lens. Once the CNP was affixed to the amplifier headstage, its conductive carbon tip could penetrate the cell membrane to provide a nanoscale electrical conduit for accessing the intracellular environment (Figure 1C).

To demonstrate the feasibility of carrying out electrophysiological measurements with CNPs, we measured the resting membrane potential (RMP) of the mouse hippocampal cell line HT-22 and the subsequent potential variations caused by adding pharmacological agents to the cell bath. Mammalian cells can exhibit RMPs ranging from −30 to −75 mV as a result of ion concentration differences between the intra- and extracellular domains. The electrical potential across the cell membrane can be estimated by considering the concentration differences of membrane-permeant monovalent ions using the Goldman equation[16]

$$E_m = \frac{RT}{F}\ln\left(\frac{P_{K^+}[K^+]_o + P_{Na^+}[Na^+]_o + P_{Cl^-}[Cl^-]_o}{P_{K^+}[K^+]_i + P_{Na^+}[Na^+]_i + P_{Cl^-}[Cl^-]}\right) \quad (1)$$

where R is the ideal gas constant, T is the temperature, F is the Faraday constant, P_{ion} is the permeability of the ion, and $[ion]_o$ and $[ion]_i$ are, respectively, the concentrations of the ion outside and inside the cell. Since membranes of mammalian neurons are significantly more permeable, under normal conditions, to potassium ions than sodium ions and chloride ions,[17,18] the Goldman equation simplifies to the Nernst equation

$$E_{m,K^+} = \frac{RT}{F}\ln\left(\frac{[K^+]_o}{[K^+]_i}\right) \quad (2)$$

Using the Nernst equation, we estimate a cell submerged in Hank's balanced salt solution (HBSS) ($[K^+]_o/[K^+]_i$ = 6 mM/130 mM) at room temperature (20 °C) would have a K^+-governed membrane potential of

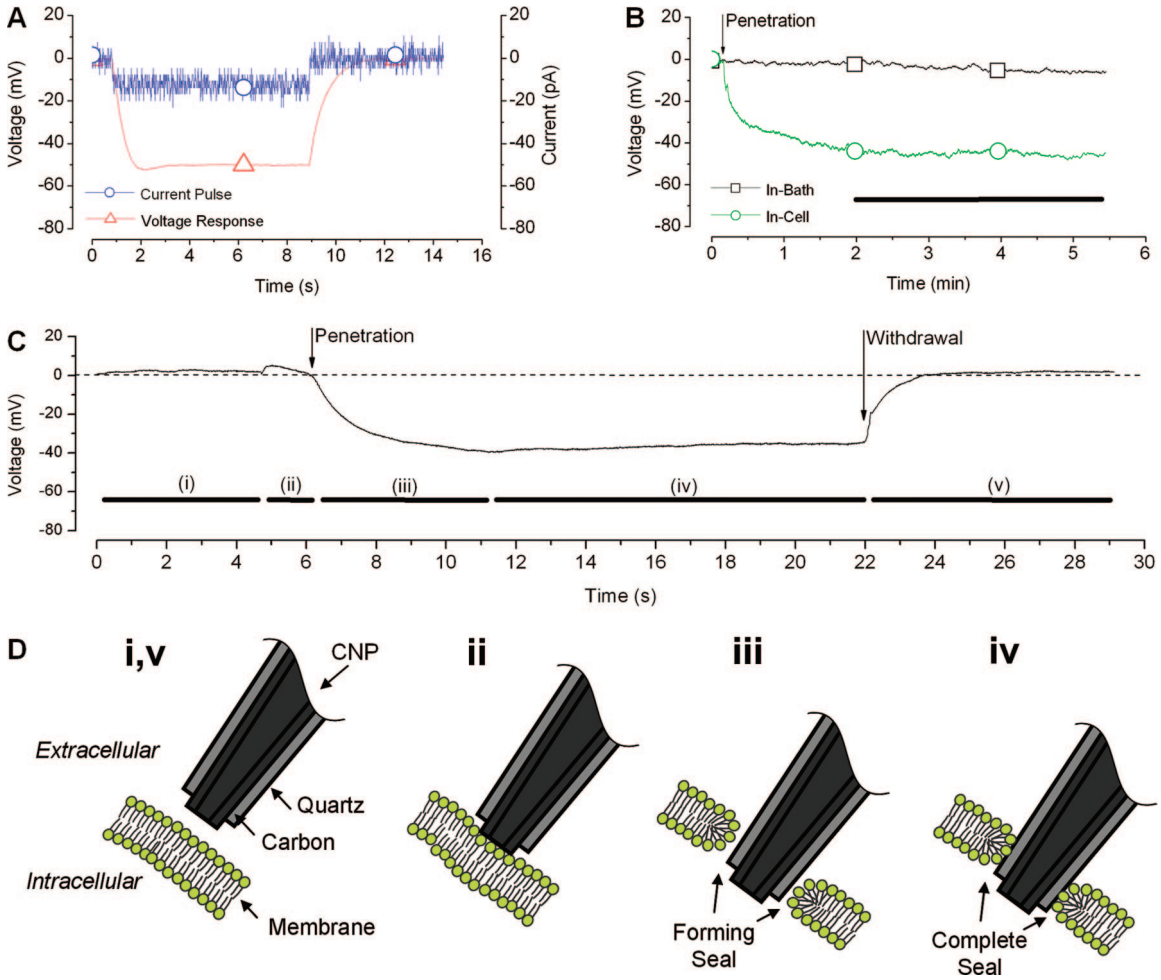

Figure 2. Measuring cell membrane potentials with CNPs. (A) Typical CNP voltage response (−50 mV) to a −10 pA current pulse measured *versus* an Ag/AgCl reference electrode submerged in HBSS. (B) Voltage recording illustrating stable electrode performance (negligible drift over time, horizontal bar region) for an in-bath and in-cell CNP. (C) Changes in electrical potential during a typical electrophysiology experiment showing both penetration and withdrawal of a CNP from the cell (arrows). Horizontal bars below the trace indicate the position of the CNP in relation to the cell as illustrated in (D). (D) Cross-section schematic illustrating the position of a CNP relative to the cell: (i) outside the cell; (ii) touching the cell membrane; (iii) forming a high-resistance seal with the cell membrane; (iv) measuring the resting membrane potential; and (v) outside the cell.

roughly −78 mV. By introducing pharmacological agents to the cell bath that modify the intracellular and extracellular ion concentrations, we expect to alter the cell membrane potential and measure the variations with CNPs.

RESULTS AND DISCUSSION

Intracellular Recording with Carbon Nanopipettes. Figure 2A shows a typical CNP-measured voltage (−50 mV) in response to a small square current pulse of −10 pA when the CNP is immersed in the HBSS. The corresponding effective resistance (5 GOhm) is attributed to the extremely small area of the carbon surface exposed to the solution and the need to overcome the solid−liquid junction impedance.[19] By fitting the response lag with an exponential decay for an RC circuit, we estimate that the entire measurement system has an effective capacitance of 200 pF with a time constant of 660 ms, which is comparable to systems utilizing electrolyte-filled glass electrodes.

Next, we assessed whether CNPs were capable of measuring the membrane potentials of cells with stability and low drift during a long-time recording. Our cell potential measurements were carried out with a high impedance amplifier and at zero current. In this way, we precluded electrochemical issues which arise for submicrometer-sized electrodes.[20] In other words, we anticipate that the CNPs behave like perfectly polarizable (blocking) electrodes.

Figure 2B illustrates the drift behavior of a CNP electrode during in-bath and in-cell voltage recordings over several minutes. As indicated in Figure 2B (horizontal bar region), the in-bath and in-cell CNP recordings have negligible drift over several minutes. Although negligible drift is typical in our experience, we observed drift on occasion as high as 1.25 mV/min in the negative direction. Over the several minutes after penetrating HT-22 cells, CNPs measured RMPs of −61.5 ± 2.97 mV (mean ± SEM; $n = 26$) from stable signals with noise ranging from 1.1 to 1.6 mV rms.

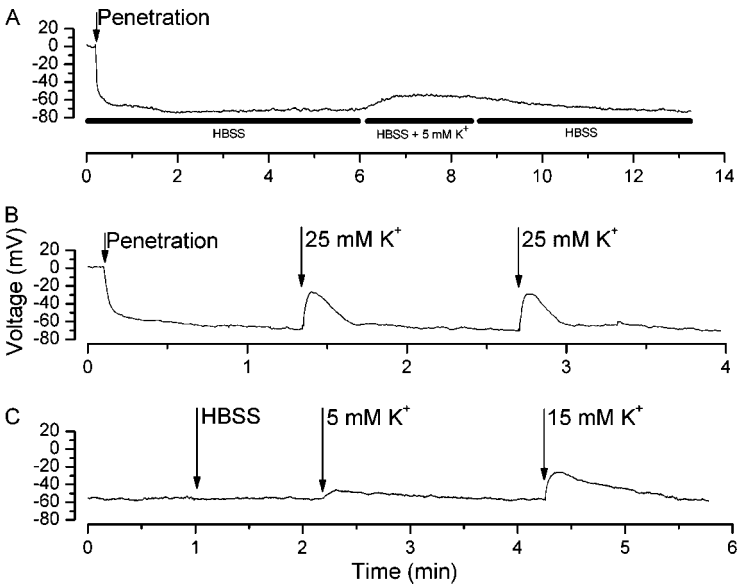

Figure 3. CNP-recorded variations in membrane potential during ionic enrichment. (A) Variations as a function of time during a short perfusion interval (~2 min, middle horizontal bar) with K^+-enriched HBSS (additional 5 mM K^+). (B) Variations as a function of time during the repetitive K^+ enrichment of HBSS (additional 25 mM K^+). (C) Variations as a function of time during the administration of normal HBSS and the varied K^+ enrichment of HBSS (additional 5 and 15 mM K^+).

Figure 2C shows CNP-measured potential variations as a function of time as a CNP approached, penetrated, and withdrew from an HT-22 cell. Figure 2D schematically depicts the position of the CNP relative to the cell. Regions (i)−(v) in Figure 2C are cross-referenced with the CNP positions in Figure 2D. Once the CNP was lowered into the bath solution and approached the adherent cell, the CNP potential was nulled (Figure 2C,D(i)). Before cell penetration, a slight potential increase (+5 mV) indicated close approach and contact between the CNP and the cell membrane (Figure 2C,D(ii)). When the CNP penetrated the cell membrane, as indicated by the arrow in Figure 2C, there was a steep drop in the potential. As the ruptured cell membrane formed a high-resistance seal with the quartz exterior of the CNP (Figure 2C,D(iii)), the voltage drop asymptoted and became nearly level after approximately 3 s. A successful CNP current-clamp was evident upon measuring a stable RMP (E_{RMP} = −35 mV) (Figure 2C,D(iv)). After a short but successful current-clamp, the CNP was withdrawn from the cell, as indicated by the arrow in Figure 2C, and the potential returned to its extracellular value of zero (Figure 2C,D(v)).

Recording Cellular Responses to Ionic Enrichment. Since the cell membrane is highly permeable to potassium ions (K^+), an increase or decrease in extracellular K^+ concentration will, respectively, cause a resting cell to depolarize (membrane potential becoming more positive) or hyperpolarize (membrane potential becoming more negative). Utilizing CNPs, variations in membrane potential were monitored over tens of minutes. Figure 3A is a recording of membrane potential from an HT-22 cell during perfusion intervals with normal HBSS and K^+-enriched HBSS (additional 5 mM K^+). Subsequent to penetrating the cell with a CNP and measuring a stable RMP under normal HBSS perfusion (E_{RMP} = −72 mV), the cell was perfused with K^+-enriched HBSS, which resulted in a 15 mV depolarization. After approximately 2 min at higher extracellular K^+, the cell was perfused with normal HBSS and the cell slowly returned to its RMP.

Next, we used a CNP to measure changes in membrane potential during repetitive extracellular administration of KCl (Figure 3B). After penetrating the cell, as indicated by the arrow in Figure 3B, the CNP measured a stable RMP under normal HBSS perfusion (E_{RMP} = −68 mV). Adding KCl to the cell bath (additional 25 mM K^+) produced a transient, K^+-enriched HBSS environment, which resulted in a 40 mV depolarization. Under constant perfusion in normal HBSS, the membrane potential returned to its original value after ~30 s. The results were reproducible with high fidelity.

Figure 3C is a representation of potential variations as a function of time during the administration of HBSS and the varied K^+ enrichment of HBSS (additional 5 and 15 mM K^+). As expected and illustrated in Figure 3C, the addition of normal HBSS did not change extracellular K^+ concentration and therefore did not affect the RMP (E_{RMP} = −57 mV). In contrast, adding KCl to the cell bath (additional 5 mM K^+) produced a transient, K^+-enriched HBSS environment, which resulted in a 10 mV depolarization. As normal HBSS perfusion brought the bath back to its initial K^+ concentration, the cell returned to its RMP in ~90 s. Likewise, adding more KCl to the cell bath (additional 15 mM K^+) resulted in a 30 mV depolarization before returning to its RMP in ~90 s.

The membrane potentials of HT-22 cells over various extracellular K^+ concentrations were consistent with predictions based on the Nernst equation. Figure 4 compares the experimental data (symbols) measured with CNPs and Nernst predictions (dotted lines) of cell membrane potentials as a function of extracellular K^+ concentration. The various symbols and lines represent cells in HBSS having different RMPs. CNP-recorded RMPs of HT-22 cells were in agreement with the K^+-governed membrane potentials predicted by the Nernst equation (E_{m,K^+} = −78 mV). Moreover, CNP-measured potential variations due to changes in extracellular K^+ concentration were in good agreement with Nernst predictions.

Recording Cellular Responses to Pharmacological Stimuli. In addition to monitoring predictable cell membrane potential changes caused by ionic enrichment, we utilized CNPs to electrically record cell responses to pharmacological stimuli. We administered γ-aminobutyric acid (GABA), a principal inhibitory neurotransmitter in the

mammalian central nervous system which acts as an agonist for the membrane-bound $GABA_A$ receptor. When GABA binds to the $GABA_A$ receptor, the cell hyperpolarizes as a result of Cl^- ion influx due to the opening of the ligand-gated Cl^- ion channel. However, the hyperpolarization can be blocked by perfusing cells with bicuculline (BIC), a competitive antagonist for the $GABA_A$ receptor which binds to the $GABA_A$ receptor and prevents it from opening even in the presence of GABA. Several reviews detailing these mechanisms exist.[21]

Figure 5a illustrates how an HT-22 cell responded when GABA was added to the cell bath (12 mM GABA in bath, arrow). The addition of GABA resulted in a 10 mV hyperpolarization (black triangles) from the RMP ($E_{RMP} = -53$ mV). Under constant HBSS perfusion, the cell returned to its RMP in 30 s. In contrast, as demonstrated in Figure 5A, administering GABA to the same cell pretreated with bicuculline (10 μM) resulted in a 5 mV hyperpolarization (red circles). The hyperpolarizing response to GABA was completely blocked (blue squares) by perfusion of BIC at a higher concentration (20 μM).

Last, we utilized CNPs to electrically record a cell response to sequential pharmacological stimulation and ionic enrichment. Figure 5B represents the opposing membrane responses to such stimuli over time. The extracellular administration of GABA (12 mM GABA in bath, arrow) resulted in a 12 mV hyperpolarization from its RMP ($E_{RMP} = -57$ mV). Once the GABA was washed away under constant HBSS perfusion, the cell returned to its RMP in 60 s. Following stabilization, the addition of KCl to the bath (additional 15 mM K^+) produced a transient, K^+-enriched HBSS environment, which resulted in a 25 mV depolarization. As excess KCl was washed away under constant HBSS perfusion, the cell returned again to its RMP after 60 s.

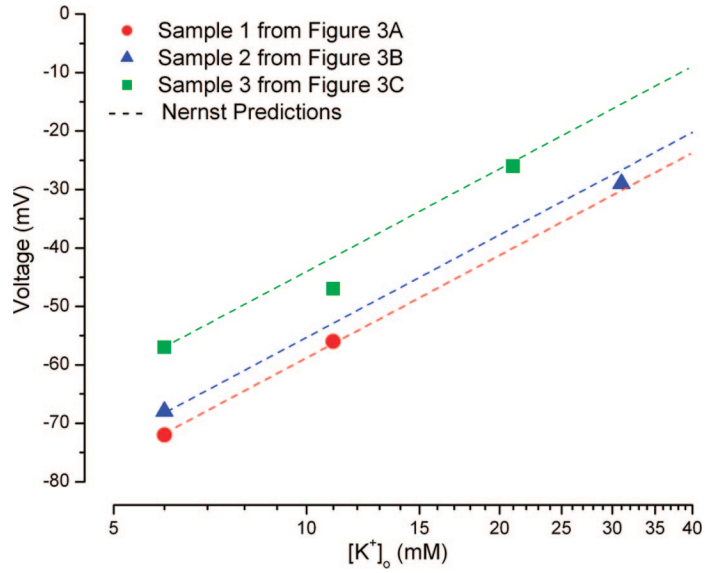

Figure 4. CNP-recorded membrane potentials of HT-22 cells as functions of the extracellular K^+ concentration. The various symbols and lines represent cells in HBSS having different RMPs. The symbols and lines correspond, respectively, to experimental data and predictions based on the Nernst equation.

SUMMARY

Traditionally, electrolyte-filled, glass-based electrodes have been used to monitor cell membrane potentials. Our work demonstrates the utility of carbon nanopipettes (CNPs) as ohmic nanoelectrodes for intracellular electrophysiological recording. CNPs recorded the electrical responses of cells to pharmacological agents, the values of which matched well with predictions from the Nernst equation. Using CNPs, we have also demonstrated that HT-22 cells hyperpolarize *via* the $GABA_A$ receptor in response to extracellular administration of GABA.

CNPs have a number of advantages over glass-based electrodes. First, they facilitate lengthy measurements without ions diffusing from the hollow of the electrode into the cell, and they are less likely to break and clog during use. Second, CNPs have the capability of facilitating concurrent intracellular injection and electric measurements, making them well-suited for multifunctional cell probing. Third, we have demonstrated that cell penetration can be sensed electrically, which can facilitate the automation of cell injection. In future work, we aim to demonstrate the CNP's multifunctional capabilities by electrically recording cellular responses to injected reagents.

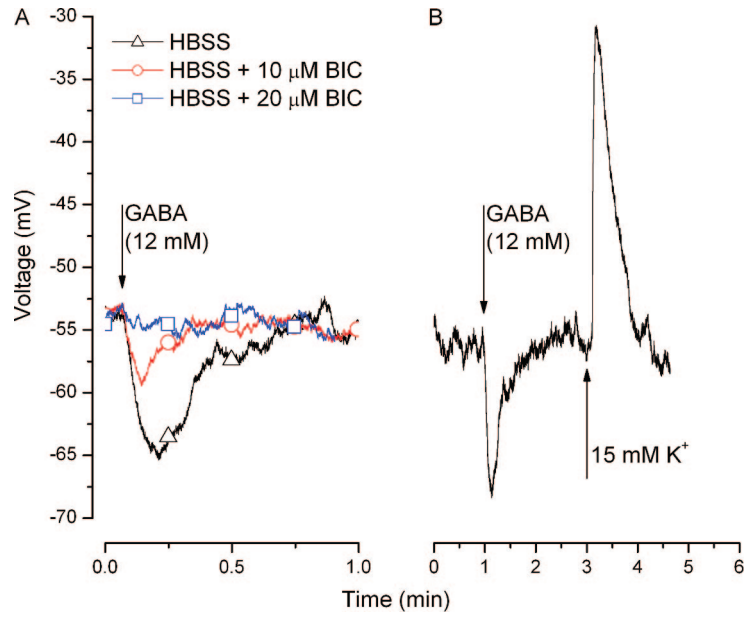

Figure 5. CNP-recorded variations in membrane potential during pharmacological stimulation. (A) Variations during the administration of GABA (12 mM, arrow) to HT-22 cells perfused in normal HBSS (black triangles), HBSS and 10 μM BIC (red circles), and HBSS and 20 μM BIC (blue squares). (B) Variations over time during the administration of GABA (12 mM, arrow) and the K^+ enrichment of HBSS (additional 15 mM K^+).

METHODS

CNP Fabrication. CNPs were fabricated using processes described previously.[11] Briefly, catalyst-laden quartz capillaries were first pulled into fine-tipped, blunt taper micropipettes. Next, the micropipettes were subjected to a chemical vapor deposition process which selectively deposits a carbon film along the entire length of the inner catalyzed surface. The thickness of the film was controlled by adjusting the deposition time. The tips were then dipped in buffered hydrofluoric acid at room temperature for 30 s to expose a very short length (<1 μm) of the interior carbon nanopipe. Hundreds of CNPs with tip outer diameters ranging from 200 to 400 nm (30 nm wall thickness) were fabricated concurrently without a need for any assembly. Figure 1A,C shows, respectively, a micrograph and a schematic depiction of the CNP.

Cell Culture and Preparation. The mouse hippocampal cell line HT-22 was kindly provided by Dr. David Schubert (The Salk Institute, San Diego, CA). Cells were grown in Dulbecco's modified Eagle medium (DMEM, high glucose) supplemented with 10% fetal bovine serum (FBS) and 1% antibiotics. The cells were plated on 12 mm coverslips 48 h prior to the electrophysiology measurements. The cells on the coverslips were incubated in HBSS (with calcium and magnesium) at room temperature for 10 min prior to measurements. The coverslips were subsequently placed in an open diamond perfusion bath (Warner Instruments Corp., RC-22C) positioned on an upright microscope (Nikon eclipse E600FN, 40X water-immersion lens, Burleigh Gibraltar fixed-stage platform) located atop a vibration-isolation table. Cells were routinely perfused with HBSS at a flow rate of 1.0 mL/min.

Electrophysiology. Membrane potential measurements were recorded with an Axon AxoClamp-2A amplifier equipped with a headstage for high-resistance electrodes (Axon HS2-X0.01MU) and Digidata 1322A digitizer (Axon Instruments/Molecular Devices, Sunnyvale, CA). Experimental protocols were controlled and data acquired by a personal computer using the Clampex 8.2 software (Axon Instruments). CNPs were inserted into a standard electrode holder until the metal wire of the holder came in contact with the inner carbon film of the CNP. A slight positive pressure was applied through the holder's perfusion port to keep external solution from filling the hollow CNP by capillarity. All the electrical measurements were carried out *versus* a Ag/AgCl reference electrode submerged in HBSS in discontinuous current-clamp (DCC) mode, at zero current, with no capacitance compensation. The CNP potential was nulled (± 2 mV) with the amplifier offset potential during immersion in HBSS before all electrical measurements. A micromanipulator (Narishige MHW-3) was used to slowly advance a CNP tip toward a cell until it made contact with the cell membrane (as observed by a slight positive potential) and hold it in place during the electrophysiology measurements. As observed in previous work,[15] the CNP tip penetrated into the cell $\ll 1$ μm and avoided penetrating into cell organelles. Recorded electrical measurements were not adjusted to compensate for differences in extracellular and intracellular junction potentials.

Chemicals. Potassium chloride (KCl), (−)-bicuculline methiodide (BIC), and γ-aminobutyric acid (GABA) were purchased from Sigma Chemical Co (St. Louis, MO). Hank's balanced salt solution (HBSS, with calcium and magnesium, ~6 mM K^+) was purchased from HyClone/Thermal Fischer Scientific, Inc. (Logan, UT).

Acknowledgment. This work was supported by the Nanotechnology Institute, Ben Franklin Technology Partners of Southeastern Pennsylvania. The authors would like to thank D. Schubert of the Salk Institute for kindly providing HT-22 cells, E. and C. Brailoiu of Temple University for fruitful discussions on electrophysiology, and X. Gao of Temple University for assistance with HT-22 cell culture.

REFERENCES AND NOTES

1. Pun, R. Y. K. Voltage Clamping with Single Microelectrodes: Comparison of the Discontinuous Mode and Continuous Mode Using the Axoclamp 2A Amplifier. *Mol. Cell. Biochem.* **1988**, *80*, 109–120.
2. Neher, E.; Sakmann, B. Single-Channel Currents Recorded from Membranes of Denervated Frog Muscle Fibres. *Nature* **1976**, *260*, 799–802.
3. Graham, J.; Gerald, R. W. Membrane Potentials and Excitation of Impaled Single Muscle Fibers. *J. Cell. Comp. Physiol.* **1946**, *28*, 99–117.
4. Ling, G.; Gerald, R. W. The Normal Membrane Potential of Frog Sartorious Fibers. *J. Cell. Comp. Physiol.* **1949**, *34*, 383–396.
5. Safronov, B. V.; Vogel, W. Electrical Activity of Individual Neurons: Patch-Clamp Techniques. In *Modern Techniques in Neuroscience Research*; Windhorst, U., Johansson, H., Eds.; Springer-Verlag: Berlin, Heidelberg, 1999; pp 146−158.
6. Laforge, F. O.; Carpino, J.; Rotenberg, S. A.; Mirkin, M. V. Electrochemical Attosyringe. *Proc. Natl. Acad. Sci. U.S.A.* **2007**, *104*, 11895–11900.
7. Kleps, I.; Miu, M.; Craciunoiu, F.; Simion, M. Development of the Micro- and Nanoelectrodes for Cells Investigation. *Microelectron. Eng.* **2007**, *84*, 1744–1748.
8. Held, J.; Gaspar, J.; Koester, P. J.; Tautorat, C.; Cismak, A.; Heilmann, A.; Baumann, W.; Trautmann, A.; Ruther, P.; Paul, O. Microneedle Arrays for Intracellular Recording Applications. *IEEE 21st International Conference on Micro Electro Mechanical Systems* **2008**, 268–271.
9. Yum, K.; Cho, H. N.; Hu, L.; Yu, M.-F. Individual Nanotube-Based Needle Nanoprobes for Electrochemical Studies in Picoliter Microenvironments. *ACS Nano* **2007**, *1*, 440–448.
10. Sun, P.; Laforge, F. O.; Abeyweera, T. P.; Rotenberg, S. A.; Carpino, J.; Mirkin, M. V. Nanoelectrochemistry of Mammalian Cells. *Proc. Natl. Acad. Sci. U.S.A.* **2007**, *105*, 443–448.
11. Schrlau, M. G.; Falls, E. R.; Ziober, B. L.; Bau, H. H. Carbon Nanopipettes for Cell Probes and Intracellular Injection. *Nanotechnology* **2008**, *19*, 015101.
12. Fischer, J. E. Carbon Nanotubes: Structure and Properties. In *Nanotubes and Nanofibers*; Gogotsi, Y., Ed.; CRC Press: Boca Raton, FL, 2006; pp 58−70.
13. Yang, W.; Thordarson, P.; Gooding, J. J.; Ringer, S. P.; Braet, F. Carbon Nanotubes for Biological and Biomedical Applications. *Nanotechnology* **2007**, *18*, 412001.
14. Kim, B. M.; Murray, T.; Bau, H. H. The Fabrication of Integrated Carbon Pipes with Sub-Micron Diameters. *Nanotechnology* **2005**, *16*, 1317–1320.
15. Schrlau, M. G.; Brailoiu, E.; Patel, S.; Gogotsi, Y.; Dun, N. J.; Bau, H. H. Carbon Nanopipettes Characterize Calcium Release Pathways in Breast Cancer Cells. *Nanotechnology* **2008**, *19*, 325102.
16. Goldman, D. E. Potential, Impedance, and Rectification in Membranes. *J. Gen. Physiol.* **1943**, *27*, 37–60.
17. Hodgkin, A. L.; Katz, B. The Effect of Sodium Ions on the Electrical Activity of the Giant Axon of the Squid. *J. Physiol.* **1949**, *108*, 37–77.
18. Baker, P. F.; Hodgkin, A. L.; Shaw, T. I. Replacement of the Axoplasm of Giant Nerve Fibres with Artificial Solutions. *J. Physiol.* **1962**, *164*, 330–354.
19. Robinson, D. A. The Electrical Properties of Metal Microelectrodes. *Proc. IEEE* **1968**, *56*, 1065–1071.
20. Yoon, Y.-H.; Shin, T.; Shin, E.-Y.; Kang, H.; Yoo, J.-S.; Park, S.-M. A Nanometer Potential Probe for the Measurement of Electrochemical Potential of Solution. *Electochim. Acta* **2007**, *52*, 4614–4621.
21. MacDonald, R. L.; Olsen, R. W. GABA-A Receptor Channels. *Annu. Rev. Neurosci.* **1994**, *17*, 569–602.